Fast formation of low-defect-density tethered bilayers by fusion of multilamellar vesicles

Article *in* Biochimica et Biophysica Acta · January 2017

DOI: 10.1016/j.bbamem.2017.01.015

Biochimica et Biophysica Acta 1859 (2017) 669–678

Contents lists available at ScienceDirect

Biochimica et Biophysica Acta

journal homepage: www.elsevier.com/locate/bbamem

Fast formation of low-defect-density tethered bilayers by fusion of multilamellar vesicles

Tadas Ragaliauskas [a,1], Mindaugas Mickevicius [a,1], Bozena Rakovska [a], Tadas Penkauskas [a], David J. Vanderah [b], Frank Heinrich [c,d], Gintaras Valincius [a,*]

[a] Institute of Biochemistry, Vilnius University, Sauletekio 7, Vilnius LT-10257 , Lithuania
[b] Institute for Bioscience and Biotechnology Research, Rockville, MD 20850, USA
[c] Center for Neutron Research, National Institute of Standards and Technology, Gaithersburg, MD 20899, USA
[d] Department of Physics, Carnegie Mellon University, Pittsburgh, PA 15213, USA

ARTICLE INFO

Article history:
Received 13 October 2016
Received in revised form 19 December 2016
Accepted 10 January 2017
Available online 12 January 2017

Keywords:
Phospholipid membranes
Tethered bilayers
Electrochemical impedance
Alpha hemolysin
Neutron
Vesicles

ABSTRACT

A facile and reproducible preparation of surface-supported lipid bilayers is essential for fundamental membrane research and biotechnological applications. We demonstrate that multilamellar vesicles fuse to molecular-anchor-grafted surfaces yielding low-defect-density, tethered bilayer membranes. Continuous bilayers are formed within 10 min, while the electrically insulating bilayers with $<0.1\ \mu m^{-2}$ defect density can be accomplished within 60 min. Surface plasmon resonance spectroscopy indicates that an amount of lipid material transferred from vesicles to a surface is inversely proportional to the density of an anchor, while the total amount of lipid that includes tethered and transferred lipid remains constant within 5% standard error. This attests for the formation of intact bilayers independent of the tethering agent density. Neutron reflectometry (NR) revealed the atomic level structural details of the tethered bilayer showing, among other things, that the total thickness of the hydrophobic slab of the construct was 3.2 nm and that the molar fraction of cholesterol in lipid content is essentially the same as the molar fraction of cholesterol in the multilamellar liposomes. NR also indicated the formation of an overlayer with an effective thickness of 1.9 nm. These overlayers may be easily removed by a single rinse of the tethered construct with 30% ethanol solution. Fast assembly and low residual defect density achievable within an hour of fusion makes our tethered bilayer methodology an attractive platform for biosensing of membrane damaging agents, such as pore forming toxins.

1. Introduction

Artificial solid-supported phospholipid bilayers are models that allow the investigation of interactions between proteins (peptides) and biological membranes. The first supported bilayer systems were assembled on solid substrates such as glass and silica [1]. Later, methodologies were developed for metals [2] and metal oxide substrates [3]. Various experimental techniques were employed [4] for the formation of bilayers on surfaces, such as Langmuir-Blodget film transfer [1], spin-coating, solvent exchange [5], and adsorption of mixed micelles [6] or liposome fusion [7]. While the quality of the bilayers depended on the surface nature [8] and the self-assembly conditions [9,10], generally, these methodologies produced freely-suspended, continuous bilayers, as evidenced by the surface plasmon resonance (SPR) and quartz crystal microbalance with dissipation (QCM-D) [9], atomic force microscopy (AFM) [11], neutron reflectometry (NR) [12] and fluorescence techniques [13].

Vesicle fusion is one of the few bilayer methodologies, which allows real-time observation and monitoring of the bilayer formation [14–16]. Various lipid compositions, including proteasomes and membranes derived from cells, may be may be fused to a solid surface [15,17]. Typically, the techniques such as SPR [18,19] or (QCM) [14,15,17] are utilized for monitoring of bilayer formation. On the other hand, the fluorescence imaging [1] or AFM [10,11] are the methods of choice to observe the bilayer lateral heterogeneity. Neutron reflectometry is the technique used to determine lipid material distribution along the normal to a surface on the near-atomic resolution. It gives information about the parameters of solid supported bilayers, such as thickness of the bilayer, area per lipid molecule, the position of membrane components such as cholesterol, and others [20,21]. According to neutron reflectometry data, the distance between solid support and the phospholipid headgroups is small, typically, <1.0 nm [22].

While vesicle-fused, freely-suspended membranes can provide a variety of functional membrane models for protein incorporation studies, they exhibit three major drawbacks. First, the distance between solid

* Corresponding author.
E-mail address: gintaras.valincius@bchi.vu.lt (G. Valincius).
[1] These authors contributed equally.

http://dx.doi.org/10.1016/j.bbamem.2017.01.015
0005-2736/

supports is rather small, potentially interfering with the reconstitution of transmembrane proteins with large intracellular domains. Second, the stability of freely-suspended membranes is poor, and the lateral integrity is relatively low. Third, patches and pinholes are abundant [23], rendering these bilayers less suitable for lateral diffusion and electrical conductance studies. The problem with a too-close-to-the-substrate positioning is resolved by providing hydrogel polymer cushions for bilayers [4,7,24]. However, lateral instability and poor electric sealing is a major obstacle precluding utilization of freely-suspended bilayers in biosensor applications, including those on polymer cushions.

Stability and electrical sealing is significantly improved upon introduction of lipidic tether molecules, covalently attached to the solid surface, that insert into the phospholipid bilayer via hydrophobic interactions thus providing molecular anchoring for surface supported structure called the tethered bilayer membranes (tBLMs). Such tethers were first introduced by Lang et al. [2,25]. A whole spectrum of different anchor compounds were developed later [26–35]. The concept of tethers was also extended to polymer cushioned bilayers [36,37].

Several methodologies are used to form tBLMs. Amongst them rapid solvent exchange (RSE) is one of the most widely used [28,33,38,39]. RSE bilayers exhibit excellent electrical sealing properties [40] and longevity [41]. The formation process is fast, but the real-time monitoring of the bilayer formation is impossible. In addition, the RSE methodology allows limited phospholipid compositions because it requires lipids forming tBLM to be soluble in the exchangeable solvent, which is not always possible; however, compositional variation may be supplemented by lipid material exchange with RSE-formed tBLMs [42].

Attempts were made to use vesicle fusion for the formation of the tBLMs [29,30,40,41,43]. Suspensions of small unilamellar vesicles are utilized to accomplish tBLMs. Complete and electrically insulating bilayers were formed only if densely-packed, mono-component SAM anchors were used [40,44]. Densely-packed constructs are similar to the hybrid bilayer membranes, which exhibit limited ability to functionally reconstitute transmembrane proteins due to dense inner leaflet [45]. Such limitations are well documented [46,47]. Vesicles can also be fused to less dense, sparse tether systems made of one [40] or two components – a hydrophobic lipidic anchor and a shorter hydrophilic backfiller. However, the electrical resistance of tBLMs deteriorates quickly with tether density [40,43]. While the measured resistance of tBLMs may not necessarily be solely determined by the number of defects (see ref. [48] for details), decreasing the tether density most likely causes increased defectiveness. Another important drawback of vesicle fusion to sparsely-populated anchors is that to achieve full surface coverage and low residual conductance (high tBLM resistance) hours of incubation in the vesicle solution are required [43,46]. From a practical standpoint fast and reproducible formation of tBLMs is needed to quickly activate tBLM-based devices, for example sensors.

To date, most of the applications in which vesicle fusion was used to accomplish supported bilayers employed mono-disperse, small unilamellar vesicle (SUV) compositions. Such choice is based on the fact that, compared to large unilamellar or multilamellar vesicles, SUV exhibit larger free energy excess, which makes them less thermodynamically stable [49]. While usage of such preparations may be justified from the thermodynamic (in)stability standpoint, no attempts so far have been made to prove that such compositions are superior in terms of the quality and reproducibility of the properties of phospholipid membranes, neither it is clear that the speed of the rupture and fusion of SUVs is superior to other aggregate forms of the lipid species. The external leaflets of large onion-like multilamellar vesicles, due to small curvature exhibit near zero bending energy [50]. This means that flat phospholipid bilayers and bilayers of multilamellar vesicles may be separated by relatively narrow free energy gap, and , as a result, transitions between those two states may be swift. Such a hypothesis is supported by the spontaneous swelling of multilamellar phospholipid films and swift formation of the multilamellar vesicles. Aiming at verifying if the reverse process, i.e., the formation of flat bilayers is feasible, in this work, we studied the fusion of the multilamellar vesicle compositions (MVC) onto a special anchor self-assembled monolayers. While fusion of MVCs may be interesting from purely theoretical standpoint, our major objective was developing a fast and reliable methodology for the formation of tBLMs. We have discovered that without compromising their integrity, tBLMs can be accomplished through vesicle fusion within <60 min on sparsely populated anchor SAMs, using MVCs that can be prepared within minutes without any special treatment such as freeze-thaw cycles or extrusion. Such bilayers exhibit low defect densities, comparable to or exceeding those achievable by RSE on the same anchor SAMs. Importantly, bilayers formed by the MVCs fusion are suitable for the reconstitution and detection of transmembrane proteins, including large multimeric, cholesterol dependent toxins, such as α-hemolysin and possibly any other membrane damaging proteins.

2. Materials and methods

2.1. Sample preparation

Gold substrates for SPR were prepared on BK7 glass slides (25 mm diameter, 1 mm thickness) obtained from AutoLab (Methorm, The Netherlands). For electrochemical impedance spectroscopy (EIS) measurements 25 by 75 mm glass slides from ThermoFischer Scientific (UK) were used. Si wafers were can be used instead of glass substrates [42]. Because the substrates were coated with a relatively thick (>50 nm) gold layer no difference in electrochemical properties can be detected. For neutron reflectometry 3″ diameter 5 mm thick n-type Si:P[100] wafers (El-Cat Inc., Ridgefield Park, NJ) were used. Before vacuum deposition of metals, the substrates, except for NR measurements, were cleaned in Nochromix™ solution (Sigma-Aldrich), rinsed thoroughly with copious amount of deionized (Mili-Q , Millipore) water and dried in a dry stream of nitrogen (99.99%) filtered through a 0.05 μm dust filter from Swagelok, Finland. Metal films: titanium (~1 nm) and gold (~50 nm for SPR, ~80 nm for EIS) were coated using the PVD 75 (Kurt J. Lesker Company, USA) magnetron sputtering system. Coating details are described elsewhere [51]. The freshly-coated Au films were immediately immersed in ethanolic 0.1 mM solutions of octadecanethiol (ODT) or 0.05 mM (total disulfide concentration) of $[HC18]S_2$ and 2-hydroxyethyl disulfide [the disulfide of β-mercaptoethanol, $(\beta ME)S_2$] of various molar ratios. $[HC18]S_2$ is the disulfide form of the molecular anchor described earlier [33]. Incubations in the $[HC18]S_2/[\beta ME]S_2$ and ODT solutions was carried out for 1 h and 4 h, respectively, then immediately washed in pure ethanol and dried in a stream of nitrogen. Samples with self-assembled monolayers then were exposed to a multilamellar solutions (vide infra) for up to a 60 min during which tBLMs were formed. The experiments with tBLMs typically started immediately after the end of formation. However, the bilayers exhibited stable electrical and optical parameters for at least 72 h.

2.2. Multilamellar vesicle compositions (MVCs)

Vesicle suspensions were prepared from 1,2-dioleoyl-*sn*-glycero-3-phosphocholine (DOPC) and cholesterol (CHOL) from Avanti Polar Lipids, Inc., USA. Molar ratio of lipids was 60% DOPC and 40% cholesterol. The lipids were dissolved in chloroform (99%, Sigma-Aldrich) to a concentration of 10 mM. Typically, an aliquot of this lipid solution (~10 mL) was transferred to a separate vial and the chloroform evaporated under a continuous flow of nitrogen until a thin, uniform lipid film formed (~15–20 min). The dried lipid film was re-suspended in buffer to a 2 mM total lipid concentration using an automatic pipette (1 mL tip) and slowly (1 cycle/s) aspirated and dispensed until the lipid film on the vial walls dispersed and the solution became milky (~300 aspiration-dispense cycles to obtain a homogenous, though, milky opaque preparation). Lipid preparations were characterized (see Supporting material data) by dynamic light scattering using a Zetasizer Nano ZS

instrument (Malvern Instruments, UK). Typically, the preparation exhibited a narrow distribution with an average size of the MVCs between 500 and 1100 nm (full width at half maximum between 30 and 80 nm). The multilamellarity of the vesicles was estimated by the release of the auto quenching dye, calcein (see Supporting material data). Average number of lamellae was found to be 35 ± 3 for MVLs with diameter 900 ± 88 nm. Thus prepared, these vesicle compositions can be stored at room temperature for 1 month. However, before each experiment the lipid mixture in buffer must be mixed again (usually, 20–30 aspiration-dispense cycles) to fully restore the functional properties.

2.3. Surface plasmon resonance (SPR)

The SPR measurements were conducted on an Autolab Twingle system (Eco Chemie B.V., The Netherlands) equipped with a flow-through cell (volume – 175 μL). The unit performs SPR spectra recording at fixed wavelength of 670 nm. It automatically follows with a millidegree resolution the position of an incidence angle (ranging from 62 to 78°), at which minimum of the reflection due to an excitation of the surface plasmon resonance is observed. Model F34 refrigerating/heating circulator (Julabo, DEU) was used to stabilize temperature at 21 ± 0.1 °C. Before each experiment, baseline in buffer solution was recorded. All measurements were carried out at stopped-flow conditions.

2.4. Electrochemical impedance spectroscopy (EIS)

Electrochemical impedance spectroscopy measurements were carried out using Zennium electrochemical workstation (Zahner GmbH, DEU). The EI spectra were recorded in a potentiostatic mode with an 10 mV ac perturbation voltage at 0 V vs Ag|AgCl|NaCl(sat), with the potential + 197 mV respective to the standard hydrogen electrode. Measurements were carried out in a 6-vial measurement block-cell described earlier (see Supporting material in [42]). Each cell had 32 mm^2 surface of the working electrode at the bottom. Measurements were carried out in the frequency range from 1 Hz to 100 kHz unless otherwise indicated. Data analysis was carried out Zview 2.8 software package Zview 2.8.

2.5. Neutron reflectometry (NR)

For neutron reflectometry, 3″ diameter n-type Si:P(100) wafers (El-Cat, Ridgefield Park NJ, USA) were used for tBLM preparation. Neutron reflectivity measurements were performed at RT with the NG7 horizontal reflectometer at the NIST Center for Neutron Research (NCNR), using a neutron wavelength of 4.75 Å. Neutron reflectivity was recorded for momentum transfer values between 0.008 and 0.25 $Å^{-1}$. tBLMs were prepared and measured using a NCNR reflectometry flow cell that allows for in situ buffer and sample exchange. Therefore, initial and subsequent measurements are all taken on the same sample footprint. NR data was collected for each condition under sequential immersion in D_2O- and H_2O-based aqueous buffers (contrasts). For each measured contrast, adequate counting statistics were obtained after ~5 h.

2.6. Neutron reflectometry data analysis

NR data was evaluated with garefl and Refl1D using a Monte-Carlo Markov chain algorithm that provides a quantitative measure of model parameter confidence limits and parameter correlations. The 1D-structural profile along the lipid bilayer normal was modeled as previously reported using a hybrid of a stratified slab model for the solid substrate (bulk silicon, the silicon oxide, the chromium, and the gold layer) and a continuous distribution model [52] for the tBLM and the lipid overlayer. Fit parameters for the stratified slabs are thickness and neutron scattering length density (nSLD) for each substrate layer, except for the bulk silicon. One global roughness fit parameter applies to all substrate interfaces. Individual sub-molecular groups implemented in the continuous distribution model of the tBLM are: (βME)S_2, tether PEG chains, tether glycerol groups, substrate-proximal and substrate-distal lipid headgroups, substrate-proximal and substrate-distal methylene and methyl chains of lipid and tether molecules. The lipidic component of the tBLM excluding tether molecules is DOPC and a variable fraction of cholesterol. Fit parameters are the bilayer hydrocarbon thickness for each bilayer leaflet, bilayer completeness, tether surface density, tether thickness, βME surface density, and the fraction of cholesterol in the tBLM excluding tether molecules. The low-coverage lipid overlayer is modeled as a floating lipid bilayer of the same composition as the substrate-distal leaflet of the tBLM using separate distributions for the substrate-proximal and substrate-distal headgroups, methylene and methyl groups. Fit parameters for the overlayer are the separation of the overlayer from the tBLM measured as the distance between the two buffer/headgroup interfaces of the nearest headgroups, one hydrocarbon leaflet thickness applied to both overlayer leaflets, and the completeness of the overlayer. One roughness fit parameter is applied to all distributions of the tBLM and the overlayer.

3. Results

3.1. SPR response to the fusion of MVCs to ODT and (βME)S_2 monolayers

Fig. 1 displays SPR traces of the formation of monolayer and bilayer by fusion of 100% DOPC MVCs on hydrophobic ODT and hydrophilic (βME)S_2 surfaces. In accord to previous studies [18], on the hydroxyl-terminated SAMs, fusion produces a layer twice as thick as that on the hydrophobic ODT surface. Near saturation is achieved within 400–500 s and around 1000 s on ODT and (βME)S_2, respectively. In all cases, weakly adsorbed material is observed which can be washed off the surfaces by flushing the cell with pure buffer (arrows in Fig. 1). The average SPR angle shifts after flushing the cell at t = 1800 s was – 295 ± 4.2 m° (10 measurements) on ODT and 595 ± 7 m° (6 measurements) on (βME)S_2 [the SPR response ratio is 1:2 (within 1% error)].

3.2. SPR response to the formation of tethered bilayer via interaction with MVCs

Vesicle fusion was directly observed by SPR. The addition of 60% DOPC/40% CHOL MVCs triggered an immediate SPR signal increase (Fig. 2). The amplitude of the SPR signal variation was dependent on the composition of the mixed (HC18)S_2/(βME)S_2 SAMs (Fig. 2).

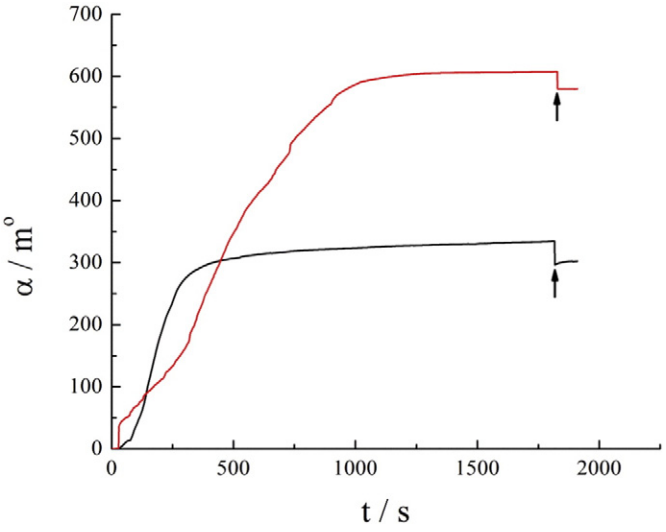

Fig. 1. SPR monitoring of lipid (DOPC) layers formation on self-assembled monolayers of: black curve – ODT; red curve – (βME)S_2 upon exposure to MVC liposome preparation. Arrows indicate initiation of a wash with buffer.

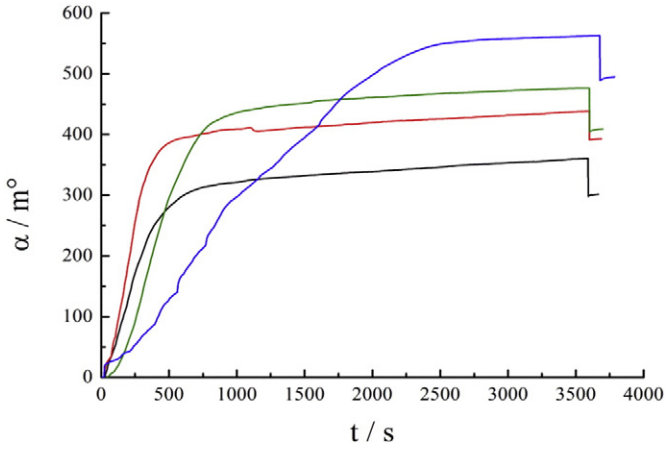

Fig. 2. SPR monitoring of 60% DOPC/40% CHOL tBLM formation on $(HC18)S_2/(\beta ME)S_2$ SAMs: black curve – 70% $(HC18)S_2$; red curve – 50% $(HC18)S_2$; green curve – 30% $(HC18)S_2$; blue curve – 10% $(HC18)S_2$. Total lipid concentration in MVCs – 1 mM. Sharp step after t = 3600 s corresponds to a rinsing of the cell with vesicle free-buffer.

Saturation typically occurs within 500–750 s, with the exception for 10% $(HC18)S_2$ anchor SAM, for which tBLM formation occurred over a significantly longer period of time (>2000 s). In all cases, flushing of the system with a vesicle-free buffer resulted in a reduction of the SPR signal by 15–20% suggesting presence of loosely-attached phospholipids.

3.3. Neutron reflectometry of tethered lipid bilayer

Neutron reflectometry curves are presented in Fig. 3 that were obtained for D_2O and H_2O bulk solvent contrasts after fusion of 60% DOPC/40% CHOL MVCs to a 30% $(HC18)S_2$/70% $(\beta ME)S_2$ SAM and after flushing the NR cell with vesicle-free buffer containing 30% ethanol. As follows from Fig. 3A, the reflectivity curve changes before and after flushing are clearly observed in the D_2O medium, predominantly in Q range between 0.02 and 0.10 $Å^{-1}$, while reflectivity curve changes obtained in H_2O are minimal. Calculated neutron scattering length density (nSLD) variations are shown in Fig. 3B. A set of the modeling parameters that is obtained from the fitting of the neutron reflectivity curves to a model is summarized in Table 1. The bilayer is 100 ± 0.1% complete and it is separated from the surface by a 11.8 ± 0.4 Å thick water filled reservoir. The total thickness of the hydrocarbon sheets is close to 32 Å. The molar fraction of cholesterol in the exchangeable lipid part of the tBLM is 39%, which is close to a composition (40% CHOL) of the MVCs used. In general, both the nSLD profile and structural parameters are close to earlier obtained in a similar molecular anchor system [33] with one exception. Separated by approximately 32 Å from the distal leaflet of the bilayer membrane a dip of the nSLD is observed under D_2O contrast conditions. This dip disappears after rinsing the measurement sample with the vesicle-free buffer containing 30% ethanol. Because there is no other loose organic material in the systems, it is natural to associate this dip with a floating, incomplete (see Table 1), lipid overlayers that are formed during fusion of the MVCs. The thickness of the overlayer is 19.0 ± 0.8 Å.

3.4. Evolution of EI spectra upon fusion of multilamellar vesicles to anchor SAMs

Injection of MVCs into the cell triggers specific EI spectral changes. Two representations of the evolution of the EIS spectra, Cole-Cole and Bode plots, are presented in Fig. 4. The initial EI curve of the anchor monolayer containing 50% $(HC18)S_2$ comprise an almost perfect semicircular feature, approaching and bouncing off near 7.4 $\mu F/cm^2$ on the Cole-Cole graph abscissa in the low frequency range. The injection of the liposome preparation into the cell immediately triggers the EI spectral changes. In particular, the large capacitive semicircle (Fig. 4A) starts

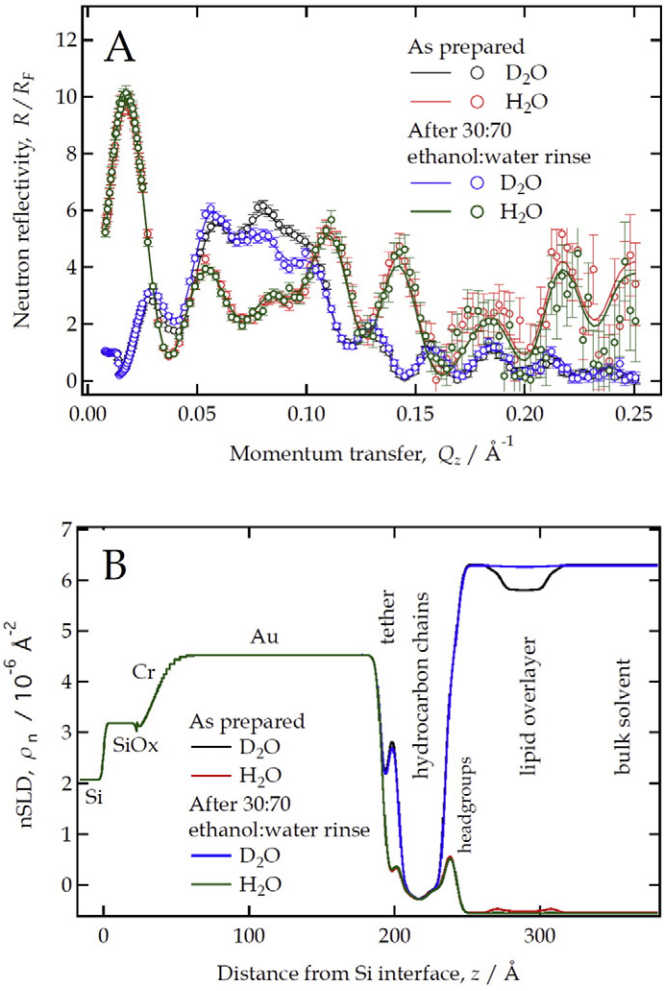

Fig. 3. Neutron reflectometry data. (A) - reflectivity curve observed after 30 min of incubation in multilamellar 60% DOPC/40% CHOL vesicle preparation (red), and after flushing the system with the vesicle-free buffer (black). (B) – Neutron scattering length distributions calculated from the curves in pane (A). Anchor monolayer was 30% $(HC18S)_2$/70% $(\beta ME)S_2$ SAM.

Table 1
Median fit parameter values and 68% confidence limits as obtained from a simultaneous fit to all measured NR data sets using a Monte Carlo Markov chain-based global optimization. Shared fit parameters between the two measured conditions are indicated using merged table cells across columns.

Fit parameter	As-prepared tBLM	tBLM after ethanol rinse
Molar fraction of tether hydrocarbon chains in substrate-proximal lipid leaflet	0.75 ± 0.18	
Number of βME molecules per tether molecule	3.0 ± 0.9	
Thickness of sub-membrane space	11.8 ± 0.4	
Thickness of hydrocarbon chains in substrate-proximal lipid leaflet/Å	14.4 ± 0.7	15.1 ± 0.6
Thickness of hydrocarbon chains in substrate-distal lipid leaflet/Å	17.6 ± 0.4	17.0 ± 0.4
Molar fraction of cholesterol in non-tether lipid component of tBLM	0.39 ± 0.02	
Bilayer completeness	1.00 ± 0.01	1.00 ± 0.01
Lipid overlayer separation to substrate-proximal bilayer/Å	19.2 ± 0.8	
Lipid overlayer thickness/Å	19.0 ± 1.2	
Lipid overlayer completeness/Å	0.067 ± 0.003	0.003 ± 0.002

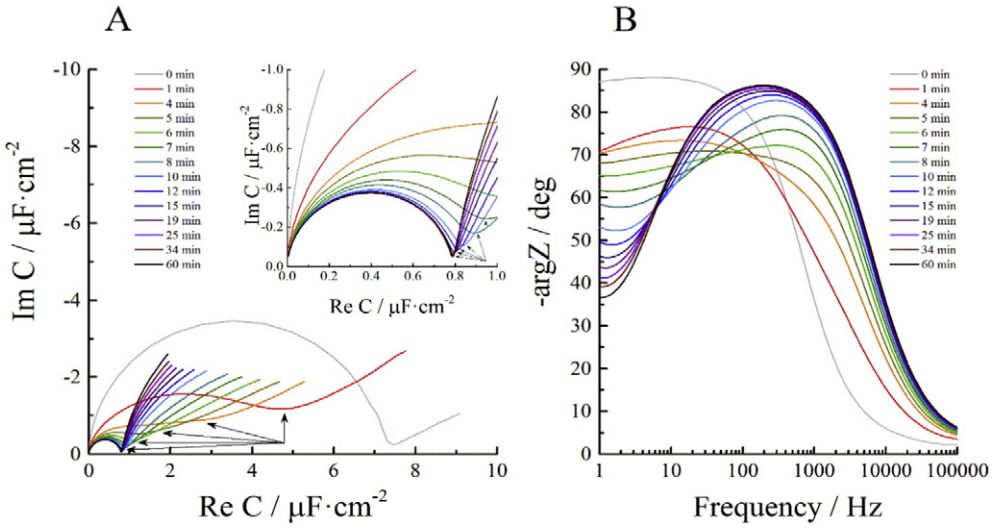

Fig. 4. Variation of the complex capacitance EIS (A) and impedance Bode (B) plots during tBLM formation on 50% $[HC18S]_2$ SAM. Inset shows enlarged high frequency part of the complex capacitance plot. Legend labels show time elapsed from the injection of MVCs into the cell. Lipid composition: 60% DOPC/40% CHOL. Total lipid concentration in MCV – 1 mM. Arrows indicate movement trajectory of the shallow minimum of the complex capacitance. Frequency range from 1 to 100,000 Hz.

shrinking and eventually, at around 10th minute of the fusion process, transforms into the semicircle with the diameter approaching 0.80 ± 0.02 μF/cm^2. Also, the formation of a second, larger arch starts emerging. Along with the changes in the Cole-Cole EI plots, the Bode plot shown in Fig. 4B indicates the formation of a pronounced minimum of the negative-of-the-impedance phase vs frequency curve at around 1 Hz. The position of the minimum on the frequency scale was sensitive to the $(HC18)S_2$ anchor density moving towards higher frequencies as the density of the $(HC18)S_2$ decreased.

3.5. EI spectral responses of tBLMs to rinsing with ethanol solution

As in the NR experiments subtle changes in EIS spectra were observed upon rinsing the tBLM with 30% ethanol/water mixture. Changes were especially visible in tBLM samples exhibiting depressed high frequency semicircular parts of the EI curve. Fig. 5 illustrates the effect. It is obvious that rinsing restores the EIS spectra to a near perfect semicircular shape.

3.6. α-Hemolysin reconstitution into MVCs fused tBLMs

α-Hemolysin is a membrane damaging protein that assembles into a heptamer, water-filled pore upon reconstitution. It was shown earlier that this protein can be reconstituted into various composition tBLMs [42,45,47,53]. To test the biological relevance of MVCs-fused tBLMs we challenged 60% DOPC/40% CHOL tBLM with 100 nM solution of α hemolysin in NaCl + phosphate buffer at pH = 4.4. Fig. 6 displays several EIS curves in the complex capacitance and Bode (phase) representations at different time intervals. The reconstitution of α-hemolysin into phospholipid bilayer at pH = 4.4 is rather facile process [53] so changes in the EI spectra are already visible after 5 min after the injection of the protein. The spectral curves exhibit clear "north west" shift of the minimum in the complex capacitance coordinates (Fig. 6A), while in the Bode coordinates two minima appear. We note that the Bode spectra in Fig. 6B are presented in the solution resistance-subtracted format. This was done to avoid unwanted effects of the solution resistance on the position of the negative of the phase minimum. Upon increasing exposure time, the low frequency minimum merges into the other one located in the higher frequency domain, and after 60 min a single minimum is located at 1100 Hz (Fig. 6B). Without the subtraction the minimum on the 60 min curve in Fig. 6B is barely visible.

4. Discussion

4.1. Quantification of the SPR response

To quantify the amount of the lipid material that is transferred from MVCs to anchor SAMs during fusion we first verified the sensitivity of the SPR using data obtained by fusion of the MVCs to non-anchoring

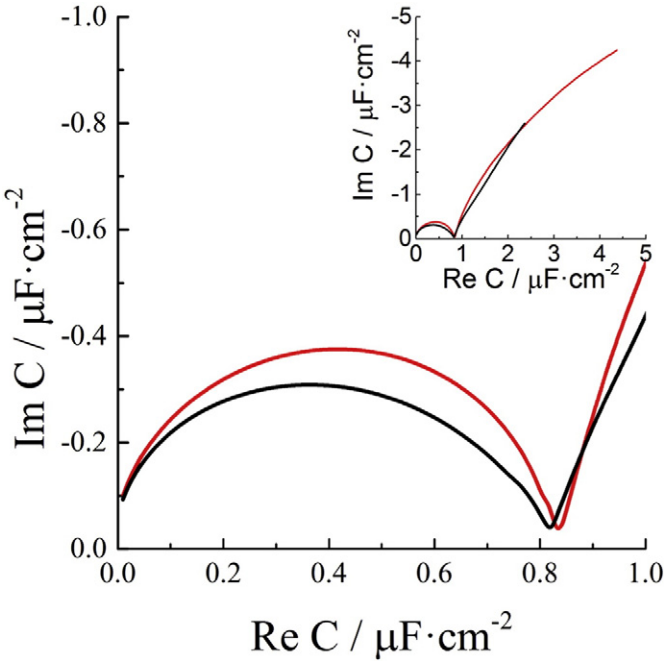

Fig. 5. Complex capacitance curves of tBLMs after 120 min fusion to 50% $(HC18S)_2$/50% $(bME)S_2$ SAM. MCV composition is 60% DOPC/40% CHOL. Black line – immediately after finishing vesicle fusion, red line – same sample after rinsing with 30% ethanol/water mixture.

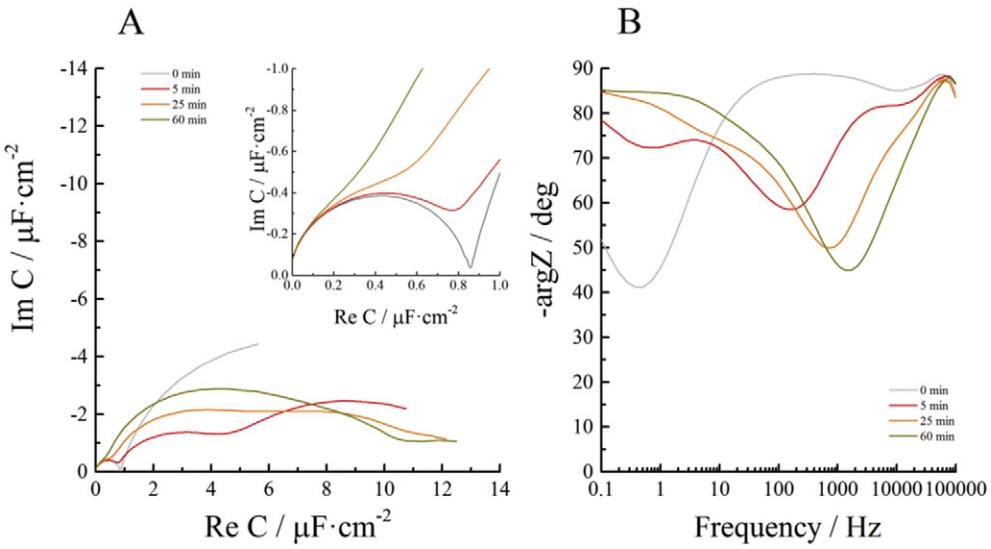

Fig. 6. Transformations of EIS spectra upon exposure of 60% DOPC/40% CHOL tBLM to 100 nM solution of α-hemolysin. A - Complex capacitance plots, B - Bode phase plots. Reconstitution buffer: 0.1 NaCl, 0.01 phosphate mixture buffered at pH = 4.4. Frequency range is from 0.1 to 100,000 Hz. From the experimental impedance curves shown in the Bode coordinates (B) the solution resistance was subtracted (see ref. [54] for details) to reveal the high frequency part of the spectra.

supports, i.e., monolayers of mercaptoethanol and ODT. For organic material localized on the surface, the amount per surface area can be estimated by the equation [55]:

$$\Delta m = d\frac{n_{biomolecule} - n_{buff}}{dn/dC} \quad (1)$$

where d is the thickness of the absorbed organic material layer, n_{org} is the refractive index of the absorption layer, n_{buff} is the refractive index of the buffer, and dn/dC is the incremental change in refractive index with concentration of the biomolecules. Eq. (1) is written under the assumption of a uniform, normal-to-the-surface material distribution within d, which holds well for monolayers. To estimate the amount of material associated with the formation of the phospholipid monomolecular layer, we used the following parameters: n_{lipids} – 1.478, n_{buff} – 1.335, dn/dC – 0.146 mL/g [56]. In the following it is assumed that n_{lipids} is independent of the tether concentration. Such an assumption is valid only if bilayer completeness is independent of tether concentration. The SPR data in Fig. 1, and NR data (Table 1) along with the EIS data analysis (vide infra) provide sufficient evidence that the bilayers are at least 99.9%, independent of tether concentration.

Based on the area per molecule data of 72 Å^2 for DOPC by Tristram-Nagle et al. [57], which is close to another data set obtained by us using NR method [33], one may expect the surface mass density of a DOPC monolayer to be $m = 181$ ng/cm^2. Using this number, as well as other constants, Eq. (1) returns an effective monolayer thickness of $d = 1.85$ nm, which can be used to estimate a SPR shift response of 290 millidegrees (m°) per monolayer of 100% DOPC, using the Winspall 3.02 software and the parameters listed in Table 2. Consequently, the SPR sensitivity is 1 m° per 0.62 ng/cm^2 of lipid material. This parameter fits well with our vesicle fusion data on pure SAMs, which does not provide anchoring of the bilayer. In particular, fusion of 100% DOPC MVCs onto ODT surface triggers the SPR shift of 295 ± 4 m° (Fig. 1), which is within 2% of the estimated value for a monolayer. On the hydrophilic (βME)S$_2$ SAMs, the shift is 597 ± 4 m° (Fig. 1), which is within 3% range for the calculated value for a bilayer. Taken together this indicates that the coefficient 0.62 ng/cm^2/m° for the SPR shift yields realistic values of vesicle-to-surface DOPC transfer.

Table 2
Parameters used to model SPR shift.

Layer	Media	Refractive index[a]	Extinction coefficients[a]	d (Å)
1	Prism	1.518	0	–
2	Titan film	2.3829	3.0414	7
3	Gold film	0.188	3.77	510
4	SAM layer	1.5	0	24
5	Lipid layer	1.478	0	18.5
6	Buffer solution	1.335	0	–

[a] Parameters for 670 nm wavelength.

4.2. Interaction with MVCs produce complete phospholipid bilayers as probed by SPR

The calculated coefficient for the SPR shift allows one to quantitate the amount phospholipid material transferred from liposomes to the surface. Importantly, both the density of the phospholipid layer proximal to a surface and the completeness of the tBLMs can be estimated. Fig. 2 and data in Table 3 indicate that the SPR angle variation during vesicle fusion is inversely proportional to the density of the anchor molecule in the anchoring SAM. This effect matches well the idea that the richer the anchor monolayer with oleoyl chains the less room is left for the lipid (in this case 100% DOPC) to populate the proximal leaflet of bilayers.

The fraction of the transferable DOPC in the proximal leaflet, X_{DOPC}, of the tBLM can estimated. Assuming the 290 m° SPR angle shift corresponds to a formation of a distal monolayer of tBLM, the rest of the SPR angle shift measures the amount of DOPC located in the proximal leaflet. Then the amount of the DOPC transferred to the proximal leaflet can be calculated from the difference between total SPR shift less 290 m°. Assuming similar dioleoyl material density in the proximal and distal leaflets, one may estimate the molar fractions of the x_{DOPC}, and x_{tether}, which

Table 3
SPR data of MVCs fusion and molar fractions of anchors and lipids in tBLMs.

Molar fraction of $(HC18S)_2$ in SAM formation mixture	10%	30%	50%	70%
SPR angle shift due to anchor SAM formation α, m°	350 ± 9	430 ± 21	530 ± 25	670 ± 15
SPR angle shift due to tBLM formation α, m°	490 ± 3	410 ± 7	400 ± 8	300 ± 4
x_{tether} (tethered oleoyl chains)	0.31	0.59	0.62	0.97
x_{DOPC} (exchangeable lipid in proximal leaflet)	0.69	0.41	0.38	0.03
Fraction of gold surface occupied by $(HC18S)_2$ anchor, x_{anchor}	7.5%	14.3%	15.0%	23.5%

is defined through the relation $x_{DOPC} + x_{tether} = 1$. Both parameters are tabulated in Table 3 as a function of the solution anchor molecule concentration. An obvious conclusion from the data in Table 3 is that the molar fraction of the anchor molecule in the anchor SAM significantly exceeds the molar fraction of the anchor molecule in solution. The fraction of the mobile lipid in inner leaflet is an important parameter in applications of tBLMs that involve the reconstitution of transmembrane proteins. As we show further, 40% of the mobile lipid, which is typically achieved in tethers formed from solutions containing 30% of anchor molecules is quite enough to functionally reconstitute even large, multimeric pore forming proteins.

While x_{tether} is significantly higher than the molar fraction of anchor in solution, the molar fraction of gold surface sites occupied by the anchor, x_{anchor}, is lower compared to its fraction in solution (Table 3). The difference between x_{tether} and x_{anchor} arise because each anchor molecule $(HC18S)_2$ terminates on the surface with the disulfide moiety that occupies lesser surface area compared to two dioleoyl chains. Consequently, relatively large amounts of backfilling molecules fill the void areas between anchor polyethylene oxide chains. Only at low tether concentration in solution and on the surface one may expect closeness of X_{anchor} to the molar fraction of anchor in solution. As the anchor concentration increases, those parameters quickly diverge because the bulky parts of the dioleoyl anchor obstructs further increase of HC18 concentration on the surface (Table 3).

4.3. Real-time monitoring of the tBLM formation by EIS attests for the integral dielectric sheet formation upon MVCs fusion

As shown in Fig. 4, tBLM assembly via MVCs fusion may be monitored in real time with EIS. Compared to SPR, the EIS has an advantage of being able not only to detect the accumulation of the phospholipid material, but also capable of sensing the development of the electrically insulating bilayer and measuring the residual defect density, as well as the formation of clusters of defects [48]. One of the most prominent changes in the impedance spectra is the transformation of the complex capacitance plots of the EIS (Fig. 4). The EIS curve of the anchor SAM before fusion of the MVCs exhibits a well-documented [33,39,51] semicircular arch shape. The low frequency leg of the arch is pointing to a value near 7.4 μF/cm^2, which is slightly higher than previously observed using RSE assembled tBLM on similar anchor SAMs [51].

Immediately, after the contact with the MVCs solution the large arch starts shrinking (Fig. 3, red orange and olive curves). Within 8–10 min of interaction, the spectra transforms into a small semicircle, with the low frequency leg now converging towards 0.80 μF/cm^2, a value close to the earlier observed capacitance of 100% DOPC tBLMs assembled via RSE [33]. Such a transformation reflects a decrease of the electrode capacitance due to coverage of the surface with the phospholipid bilayer which is equivalent to a thickness increase of the dielectric sheet on the surface. This statement can be tested by estimating the dielectric parameters of the formed construct. In particular, the following equations allow one to calculate the relative dielectric constant of the hydrocarbon sheet of the tBLM:

$$C_m = \left(C_{mH}{}^{-1} - C_H{}^{-1}\right)^{-1}, \tag{2}$$

$$\varepsilon_{hc} = \frac{C_m}{\varepsilon_0} \times d_{hc}, \tag{3}$$

in which C_{mH} is the experimentally measured (Fig. 4) capacitance of the tBLM, C_H is the experimental value of an anchor monolayer C_H = 7.4 μF/cm^2, C_m is the measured value of the of the bilayer membrane, 0.80 μF/cm^2, ε_{hc} is the vacuum constant $\varepsilon_0 = 8.85 \cdot 10^{-8}$ μF/cm, d_{hc} is the thickness of the hydrophobic sheet of the membrane, which as follows from the NR data (Table 3) is d_{hc} = 3.2 nm. Then, according to Eqs. (2) and (3), $\varepsilon_{hc} \approx 3.2$. This value is higher than $\varepsilon_{hc} = 2.32 \pm 0.2$ observed for pure DOPC monolayers on Hg surface [58]. The discrepancy may be explained by the roughness factor β, which needs to be taken into account working on solid surfaces:

$$\beta = C_{hc(measured)}/C_{hc(real)} = \varepsilon_{hc(measured)}/\varepsilon_{hc(real)} \tag{4}$$

The estimate made using the gold oxide voltammetry stripping methodology indicates that, for magnetron sputtered samples used in the current study, the roughness factor falls into the interval $\beta \in (1.30, 1.40)$. Then taking into account Eq. (4), one comes to the value $\varepsilon_{hc} \in (2.3, 2{,}5)$, which is fairly close to one reported in [58]. Based on this ε_{hc} value, one may conclude that within 8–10 min of fusion of the MCVs, the solid surface is predominantly coated with an intact phospholipid bilayer.

4.4. EIS indicate fusion propagating mechanism and allows estimation of the residual defect density

The recent theoretical analysis [48,54] also showed that qualitative EI spectral features can be used to distinguish the way defects in the tBLMs are organized as well as to estimate the residual defect densities. If in the process of accumulation defects tend to cluster, a minimum in the Cole-Cole plot that is formed in the low frequency part of the semicircular arch and the low frequency "tail" moves "north-east" as the density of defects increase [48]. Simultaneously, in the Bode plot of the impedance phase, the low frequency range minimum of the $-\arg Z$ vs frequency curve moves in the same trajectory, i.e., "north-east".

On the contrary, if defects are distributed evenly, the characteristic point in the complex capacitance plane moves "north-west", while in the Bode phase graph, the minimum moves parallel to abscissa, i.e., "east" [54].

The fusion of MVCs may be regarded as an opposite process to an accumulation of defects. So, qualitative spectral change directions should reverse. Indeed, the fusion process, as seen from Fig. 4A immediately triggers the "south-west" shift of a minimum in the complex plane (follow arrows in Fig. 4A). Initially the minimum is smeared and broad but, after >10 min, becomes clearer and sharper, discernably showing the qualitative "south-west" trend. Thus, the semicircular shape developing in the complex capacitance plots indicates the formation of an intact layer of dielectric in ≈10 min and the tBLM formation process starts with relatively small fusion centers that rapidly grows resulting in a substrate/SAM covered with a phospholipid bilayer.

EIS Bode phase diagrams confirm this conclusion. The negative of phase minimum starts developing at around 7th minute of the fusion (Fig. 4B, inset, green curve) then slowly (within 60 min) descends towards the limiting value of about $-\arg Z \approx 37$ deg, at $f_{min} \approx 1$ Hz. Modeling (details provided in the Supporting information section) of the EIS spectral response, according to theoretical framework in [48,54], allows a clear distinction of two possible scenarios. This can be done following the trajectory of the figurative point of the phase extremum, which exhibits different trajectories in cases of small and large fusion center density. Scenario one: during contact of the anchoring SAM coated substrate with the MVCs a large density of bilayer seeds are generated and the process proceeds by a gradual decrease of the density of relatively small uncovered patches (membrane defects). In such a case, at the final stages of the vesicle fusion (coverage > 90%), the impedance phase extremum will approach its final position moving almost parallel to the frequency axis (see Supporting information section for details). Scenario two: at the beginning of the fusion a relatively small number of bilayer formation seeds are formed and the process will proceed through the shrinkage of large and sparse membrane-uncovered patches. In this case the impedance phase extremum appears near $-\arg Z \approx 90$ deg and sharply descends as the vesicle fusion progresses (see the Supporting information section for details). This latter behavior is observed in the EIS features in the current study (Fig. 4B) thereby suggesting vesicle fusion by the second scenario.

The frequency at which the minimum in the Bode graph is observed allows approximate value estimates of residual defect densities achieved in the MCV fusion process, using the recently developed formalism [48] and the following equation:

$$\lg N_{def} = -0.2\ \lg r_0 + 0.93\ \lg f_{min} + A, \quad (5)$$

The constant A depends on the following parameters: d_{sub}, d_{hc}, ε_{hc}, C_H, r_0, Y_{def}, R_{sol}. From the position of the minimum $f_{min} = 1$ Hz of the Bode phase curve (Fig. 4) and assuming the following physical constants $d_{sub} = 1.18$ nm; $\rho = 100$ kΩ·cm; $d_{hc} = 3.2$ nm; $\varepsilon_{hc} = 2.3$; $r_0 = 1$ nm; $Y_{def} = 70$ pS; $C_H = 7.4$ μF/cm^2, $R_{sol} = 30$ Ω/cm^2, A = 5.6 [see ref. 48], Eq. (5) yields the residual defect density approximately ≈0.1 μm^{-2}, for tBLM formed on anchor SAM deposited from 50% $(HC18S)_2$ solutions. In Eq. (5) N_{def} only weakly depends on r_0, i.e., N_{def}, from f_{min}, will change by one order of magnitude only when r_0 changes by 5 orders of magnitude. The assumption of $r_0 = 1$ nm is possibly the lower boundary for the size of residual detects in tBLMs; therefore, it is more realistic to use $r_0 > 1$ nm, then the defect density estimate changes from $N_{def} \approx 0.1$ μm^{-2} to <0.1 μm^{-2} for 50% tether concentration tBLMs.

Analogous analysis for sparsely tethered bilayers formed on anchors deposited from 10% $(HC18S)_2$ solutions typically yielded $f_{min} \approx 70$ Hz (data in Supplemental material). Thus leads to $N_{def} < 4.8$ μm^{-2} for sparsely tethered bilayers. Defect densities obtained from the EIS data analysis allows one to estimate the surface fraction of defects. At $N_{def} < 4.6$ μm^{-2} (for 10% tether tBLMs) the surface fraction of 1 nm radial defects is $N_{def} \times S_{def} < 1.5 \cdot 10^{-5}$ (S_{def} is the area occupied by 1 defect in μm^2). So, the EIS data indicates better than 99.998% completeness of tBLMs produced by the vesicle fusion on anchors SAMs with >10% tether in solution. Similar estimates with the assumption $r_0 = 10$ nm yield surface fraction of defects $< N_{def} \times S_{def} < 1 \cdot 10^{-3}$ for 10% tether tBLMs and $N_{def} \times S_{def} < 1 \cdot 10^{-4}$ for higher tether tBLM compositions (see details in Supplementary material). Our earlier studies using AFM [59] indicates the absence of the natural defects in tBLMs with sizes above 5–10 nm, so the defect density estimates based on assumption $r_0 < 10$ nm are realistic. Based on presented data we may conclude that within 60 min fusion of the multilamellar vesicles produce >99.9% complete tBLMs for any tether concentration > 10%.

4.5. Neutron reflectometry reveals structure of tBLMs and detects formation of phospholipid overlayers during MVCs fusion

NR data shows the detailed structure of the phospholipid bilayer membrane formed by the interaction of anchor SAM with MVCs. An interesting effect was observed by NR regarding the bilayer thickness asymmetry. While the bilayers freely floating atop of the solid supports are inherently symmetrical [12], tethered bilayers (Table 1) exhibit an asymmetry in leaflet thickness. Typically monocomponent tBLMs exhibit thicker proximal hydrocarbon leaflets compared to the distal ones [33,42]. However, in the current study, in which cholesterol-loaded tBLMs were assembled, the opposite trend was observed. The distal leaflet was consistently thicker by approximately 2 Å. This observation can be explained by the well-known thickening effect of cholesterol on phospholipid bilayers. In particular, XRD and NR [12] indicate a significant thickness increase upon insertion of cholesterol into the phospholipid layers. However, in tBLMs, according to the SPR data (Table 3), proximal leaflet contains only 40% (even smaller, 25%, in NR experiments) surface unbound phospholipid, it is obvious that the proximal leaflet accommodates significantly lower cholesterol percentage compared to the distal one. Consequently, the "membrane thickening" effect is expected to manifest itself stronger in the distal leaflet, leading to a thickness asymmetry observed experimentally (Table 1).

NR allows the molar fraction of cholesterol estimate in the untethered lipid component of the tBLMs and verifies if the proportions of mixed phospholipid material is transferred to tBLMs without compositional changes. Data in Table 1 attest for the identical molar cholesterol ratio ≈ 40% in tBLMs and the MVCs from which the membrane is formed. This proves that complex lipid composition tBLMs may be quantitatively transferred during fusion from MVCs to anchor SAMs.

A most important result obtained from the NR data is the discovery of overlayers that form during MVCs fusion. As seen from data in Table 1, the overlayer is separated by approximately 2 nm from the outermost plane of the tBLM. It is covering approximately 7% of the tBLM surface, and its average thickness is significantly smaller than the total thickness of the DOPC hydrocarbon sheet. This suggests an irregular structure containing regions of highly tilted phospholipid molecules. However, these overlayers are stable in aqueous media, and may exhibit serious obstacles in tBLM applications in protein/membrane studies. For example, if the tBLM is challenged with a pore-forming protein such as α-hemolysin [41,53] its reconstitution may be obstructed and, consequently, protein-inflicted membrane damage measurements will be inaccurate. Given, the irregular nature of the overlayers, such an artifact, may significantly reduce applicability of tBLM in sensor applications that require response reproducibility. Fortunately, as the NR results demonstrate (Fig. 3B), the overlayers are readily removed by rinsing the sample with 30% ethanol solution in water. Table 1 indicates that one single flush with 30% ethanol solution reduces overlayer completeness to below 1% of the total surface area.

4.6. Overlayers affect shape of EIS curves

Deformed semicircular complex capacitance spectra are frequently obtained in tBLM systems. The deformation manifests itself as either in a depression of the semicircle or as an asymmetric arch, as seen in Fig. 5, black curve. Such spectra are typical for "as prepared" tBLMs. Interestingly, these EIS spectra have relatively short low frequency "tails", indicative of "high resistance", "low defect density" tBLMs [60]. Rinsing the "as prepared" tBLMs with 30% ethanol solution restores the symmetry of the semicircular part of the spectra, decreases depression and increases the low frequency "tails" (Fig. 5). Such behavior can be explained, taking into account NR data, by the removal of the overlayers. First, removal of overlayers unblocks sites of natural defects, thus, increasing the defectiveness of the tBLM. As modeling predicts [48,60], the defect density increase is followed by an increase of the low frequency "tails" in complex capacitance plots. Such an effect is visible in Fig. 5 (inset). Second, the presence of patches of overlayers increases the heterogeneity of the interface, therefore a depression of the complex capacitance semicircular plot is expected. Removal of overlayers restores homogeneity of the surface and as a result alleviates the depression of an arch in EIS curve, as clearly seen in Fig. 5. A convenient metrics that allows testing for the homogeneity of the surface and the absence of overlayers is the exponent of the constant phase element, which may be calculated by fitting the semicircular part of the spectra to a simple series R-CPE equivalent circuit. For "as prepared" tBLMs the exponent α exhibited values below 0.94, while after the removal of overlayers, α consistently increased above 0.98 (see the Supporting information section for details).

4.7. Functional reconstitution of aHL attests for the biological relevance of the tBLMs and their utility as biosensors

One of the prospective areas of application of tBLMs is their utility as biosensors for pore-forming membrane damaging proteins [61] or peptides. To test if tBLM assembled via MVCs-fusion are suitable for sensing of pore-forming toxin, we challenged the 60% DOPC/40% CHOL tBLM with a 100 nM solution of α-hemolysin. Injection of an α-hemolysin aliquot at pH = 4.4 immediately triggers changes in the EI spectra. The north-west shift of the minimum on the complex capacitance plot indicates a rather homogeneous distribution of the protein-induced pores [48]. Nevertheless, at the initial stages of interaction (Fig. 6, red and orange curves) clear signs of heterogeneity are visible both in the complex capacitance and Bode plots. In particular, triple semicircular features

seen in Fig. 6A and a double minimum in Fig. 6B indicates binary distribution of the defect density [60]. As the reconstitution progresses, the low frequency minimum in the Bode phase curves merge into the high frequency minimum at around 1100 Hz. Using the formalism developed in ref. [48] one may estimate the density of the α-hemolysin pores. Assuming the following physical constants $d_{sub} = 1.18$ nm; $\rho = 100$ kΩ·cm; $C_H = 7.4$ μF/cm^2, $d_{hc} = 3.2$ nm; $\varepsilon_{hc} = 3.2$; $r_0 = 1$ nm; $Y_{def} = 70$ pS; $R_{sol} = 0$ Ω and $f_{min} = 1100$ Hz we find that after 60 min of incubation, the residual defect density of α-hemolysin channels $N_{def} \approx 1000\ \mu m^{-2}$. The actual surface concentration of pores may be slightly higher because, as it is seen from Fig. 6B, the absolute value of the phase minimum, which location after 60 min reaches 1100 Hz, is several degrees higher compared to the value obtained on tBLM before reconstitution of the protein. An increase of the absolute value of the phase minimum is indicative of a cluster formation of protein pores. A cluster of pores acts a single defect, so the actual protein channel density, in our case, is $N_{def} > 1000\ \mu m^{-2}$.

5. Conclusions

In this study we demonstrate that intact tBLMs are attainable using sparsely anchored SAMs via a simple vesicle fusion process. Typically, in vesicle fusion experiments unilamellar preparations are used. Such a choice has been not justified neither theoretically nor experimentally. Our vesicle fusion protocol, in contrast to previous works, utilizes multilamellar vesicle compositions. These compositions are easy to prepare requiring no special treatments such as freeze-thaw cycles [1], multiple extrusions through the polycarbonate membranes [9,42], or multiple sonication-cooling-stirring [11]. The vesicle fusion can be accomplished on solid surfaces of a complex, including miniaturized geometry which may provide an alternative to the high quality mercury supported bilayers developed by Guidelli et al. [62]. This makes the proposed methodology as one of easiest ways to prepare tBLMs for biophysical and biochemical experiments as well as for practical applications.

Described process poses an interesting theoretical question, too. Existing studies suggest a stronger fusion propensity of smaller unilamellar vesicles. For example, on hydrophilic silica surfaces [63] unilamellar DPPC liposomes smaller than 100 nm spontaneously rupture, while liposomes larger than 160 nm do not. To our delight, even though our MVCs are significantly larger, ranging in size from approximately 500 to 1100 nm, the fusion occurred rapidly, within 10 min, and the resulting tBLMs exhibited high levels of completeness and electrical insulation. This demonstrates that the physics behind multilamellar vesicle fusion may be noticeable different compared to that for small unilamellar liposomes. While this study did not addresses in detail a difference in the kinetics of fusion of small unilamellar and large multilamellar vesicles we may assume that due to a small curvature of the external leaflets of multilamellar vesicles with near zero bending energy [50], the free energy (per lipid) gap between flat bilayers and MVCs is small. Because of a small gap, and favorable decrease of the free energy of the carbohydrogen chains of the molecular anchors upon fusion, the transitions between those two states may be swift as we observed experimentally.

Our study showed MVCs not only fuse quickly to the anchor layer but also form low residual defect density tethered bilayers. In our experiments pure DOPC bilayers assembled on anchors from 50% tether solutions exhibited defect densities of $<0.10\ \mu m^{-2}$. Residual defects determines lower sensitivity limit of the tBLM based biosensors, so low density of naturally occurring defects is crucial for practical applications of tBLM biosensors in detection of toxic agents, such as pore-forming toxins. To verify applicability of tBLM accomplished in this study we tested their capacity to reconstitute alpha hemolysin. 100 nM of α-hemolysin triggered an increase of the defect density by >4 orders of magnitude, from approximately 0.1 to $>1000\ \mu m^{-2}$, thus confirming the applicability of MVCs produced tBLMs for pore-forming toxin sensing.

Neutron reflectometry allowed us to discover overlayer formation during MVCs fusion to anchor SAMs. Such overlayers are loosely attached to tBLM and can be easily removed by 30% ethanol rinsing. tBLMs covered with overlayers exhibited a specific deformation of the EIS spectra – the depression of the semicircular part of the complex capacitance spectrum. Thus we establish that such a feature of the EIS spectra is a clear indication of the presence of overlayers. In conclusion, the proposed method of tBLM assembly is a convenient alternative to existing methods, such as RSE, to quickly assemble low-defect-density tBLMs.

Conflict of interest statement

Tadas Ragaliauskas, Mindaugas Mickevicius, Gintaras Valincius and David J. Vanderah submitted patent application to the Lithuanian Patent Office (application No.080/2015) which is related to the material presented in this manuscript. Other authors are informed about this submission. The authors declare no other conflicts of interest.

Transparency document

The Transparency document associated with this article can be found, in the online version.

Acknowledgements

This work was supported by the European Social Fund Agency Lithuania (VP1-3.1-ŠMM-08-K-01-005/KS-560000-1757). G.V. acknowledges access to the NIST Center for Neutron Research facilities and Institute of Biosciences and Biotechnology Research for providing access to the laboratory equipment. F.H. thanks for support from the Department of Commerce (MSE 70NANB13H009) and by the NIST IMS program "Precision Measurements for Integral Membrane Proteins". Certain commercial materials, equipment, and instruments are identified in this work to describe the experimental procedure as completely as possible. In no case does such an identification imply a recommendation or endorsement by National Institute of Standards and Technology, nor does it imply that the materials, equipment, or instrument identified are necessarily the best available for the purpose.

Appendix A. Supplementary data

Vesicle size measured by the dynamic light scattering, fluorescence spectroscopy-based estimate of lamellarity of multilamellar vesicles, the electrochemical impedance spectra fit data, the electrochemical impedance modeling methodology for qualitative assessment of the vesicle fusion mode and defect density estimates for various tether density tBLMs. Supplementary data associated with this article can be found in the online version, at http://dx.doi.org/10.1016/j.bbamem.2017.01.015.

References

[1] L.K. Tamm, H.M. McConnell, Supported phospholipid-bilayers, Biophys. J. 47 (1985) 105–113.
[2] H. Lang, C. Duschl, M. Gratzel, H. Vogel, Self-assembly of thiolipid molecular layers on gold surfaces - optical and electrochemical characterization, Thin Solid Films 210 (1992) 818–821.
[3] S. Gritsch, P. Nollert, F. Jahnig, E. Sackmann, Impedance spectroscopy of porin and gramicidin pores reconstituted into supported lipid bilayers on indium-tin-oxide electrodes, Langmuir 14 (1998) 3118–3125.
[4] M. Kuhner, R. Tampe, E. Sackmann, Lipid monolayer and bilayer supported on polymer-films - composite polymer-lipid films on solid substrates, Biophys. J. 67 (1994) 217–226.
[5] A.O. Hohner, M.P.C. David, J.O. Radler, Controlled solvent-exchange deposition of phospholipid membranes onto solid surfaces, Biointerphases 5 (2010) 1–8.

[6] H.P. Vacklin, F. Tiberg, R.K. Thomas, Formation of supported phospholipid bilayers, via co-adsorption with beta-D-dodecyl maltoside, Biochim. Biophys. Acta, Biomembr. 1668 (2005) 17–24.
[7] J. Spinke, J. Yang, H. Wolf, M. Liley, H. Ringsdorf, W. Knoll, Polymer-supported bilayer on a solid substrate, Biophys. J. 63 (1992) 1667–1671.
[8] E. Reimhult, F. Hook, B. Kasemo, Vesicle adsorption on SiO2 and TiO2: dependence on vesicle size, J. Chem. Phys. 117 (2002) 7401–7404.
[9] E. Reimhult, F. Hook, B. Kasemo, Intact vesicle adsorption and supported biomembrane formation from vesicles in solution: influence of surface chemistry, vesicle size, temperature, and osmotic pressure, Langmuir 19 (2003) 1681–1691.
[10] R.P. Richter, R. Berat, A.R. Brisson, Formation of solid-supported lipid bilayers: an integrated view, Langmuir 22 (2006) 3497–3505.
[11] Z.V. Leonenko, A. Carnini, D.T. Cramb, Supported planar bilayer formation by vesicle fusion: the interaction of phospholipid vesicles with surfaces and the effect of gramicidin on bilayer properties using atomic force microscopy, Biochim. Biophys. Acta, Biomembr. 1509 (2000) 131–147.
[12] H.P. Vacklin, F. Tiberg, G. Fragneto, R.K. Thomas, Composition of supported model membranes determined by neutron reflection, Langmuir 21 (2005) 2827–2837.
[13] F.F. Rossetti, M. Textor, I. Reviakine, Asymmetric distribution of phosphatidyl serine in supported phospholipid bilayers on titanium dioxide, Langmuir 22 (2006) 3467–3473.
[14] N.J. Cho, C.W. Frank, B. Kasemo, F. Hook, Quartz crystal microbalance with dissipation monitoring of supported lipid bilayers on various substrates, Nat. Protoc. 5 (2010) 1096–1106.
[15] C. Merz, W. Knoll, M. Textor, E. Reimhult, Formation of supported bacterial lipid membrane mimics, Biointerphases 3 (2008) FA41–FA50.
[16] J.M. Johnson, T. Ha, S. Chu, S.G. Boxer, Early steps of supported bilayer formation probed by single vesicle fluorescence assays, Biophys. J. 83 (2002) 3371–3379.
[17] A. Graneli, J. Rydstrom, B. Kasemo, F. Hook, Formation of supported lipid bilayer membranes on SiO2 from proteoliposomes containing transmembrane proteins, Langmuir 19 (2003) 842–850.
[18] V.I. Silin, H. Wieder, J.T. Woodward, G. Valincius, A. Offenhausser, A.L. Plant, The role of surface free energy on the formation of hybrid bilayer membranes, J. Am. Chem. Soc. 124 (2002) 14676–14683.
[19] E. Reimhult, M. Zach, F. Hook, B. Kasemo, A multitechnique study of liposome adsorption on Au and lipid bilayer formation on SiO2, Langmuir 22 (2006) 3313–3319.
[20] S.J. Johnson, T.M. Bayerl, D.C. McDermott, G.W. Adam, A.R. Rennie, R.K. Thomas, E. Sackmann, Structure of an adsorbed dimyristoylphosphatidylcholine bilayer measured with specular reflection of neutrons, Biophys. J. 59 (1991) 289–294.
[21] J.Y. Wong, J. Majewski, M. Seitz, C.K. Park, J.N. Israelachvili, G.S. Smith, Polymer-cushioned bilayers. I. A structural study of various preparation methods using neutron reflectometry, Biophys. J. 77 (1999) 1445–1457.
[22] I. Burgess, M. Li, S.L. Horswell, G. Szymanski, J. Lipkowski, J. Majewski, S. Satija, Electric field-driven transformations of a supported model biological membrane - an electrochemical and neutron reflectivity study, Biophys. J. 86 (2004) 1763–1776.
[23] J.C. Munro, C.W. Frank, In situ formation and characterization of poly(ethylene glycol)-supported lipid bilayers on gold surfaces, Langmuir 20 (2004) 10567–10575.
[24] E. Sackmann, Supported membranes: scientific and practical applications, Science 271 (1996) 43–48.
[25] H. Lang, C. Duschl, H. Vogel, A new class of thiolipids for the attachment of lipid bilayers on gold surfaces, Langmuir 10 (1994) 197–210.
[26] G. Brink, L. Schmitt, R. Tampe, E. Sackmann, Self-assembly of covalently anchored phospholipid supported membranes by use of DODA-SUC-NHS-Lipids, Biochim. Biophys. Acta, Biomembr. 1196 (1994) 227–230.
[27] A.S. Achalkumar, R.J. Bushby, S.D. Evans, Cholesterol-based anchors and tethers for phospholipid bilayers and for model biological membranes, Soft Matter 6 (2010) 6036–6051.
[28] B. Raguse, V. Braach-Maksvytis, B.A. Cornell, L.G. King, P.D.J. Osman, R.J. Pace, L. Wieczorek, Tethered lipid bilayer membranes: formation and ionic reservoir characterization, Langmuir 14 (1998) 648–659.
[29] N. Bunjes, E.K. Schmidt, A. Jonczyk, F. Rippmann, D. Beyer, H. Ringsdorf, P. Graber, W. Knoll, R. Naumann, Thiopeptide-supported lipid layers on solid substrates, Langmuir 13 (1997) 6188–6194.
[30] S.M. Schiller, R. Naumann, K. Lovejoy, H. Kunz, W. Knoll, Archaea analogue thiolipids for tethered bilayer lipid membranes on ultrasmooth gold surfaces, Angew. Chem. Int. Ed. 42 (2003) (208-+).
[31] F. Giess, M.G. Friedrich, J. Heberle, R.L. Naumann, W. Knoll, The protein-tethered lipid bilayer: a novel mimic of the biological membrane, Biophys. J. 87 (2004) 3213–3220.
[32] V. Atanasov, N. Knorr, R.S. Duran, S. Ingebrandt, A. Offenhausser, W. Knoll, I. Koper, Membrane on a chip: a functional tethered lipid bilayer membrane on silicon oxide surfaces, Biophys. J. 89 (2005) 1780–1788.
[33] R. Budvytyte, G. Valincius, G. Niaura, V. Voiciuk, M. Mickevicius, H. Chapman, H.Z. Goh, P. Shekhar, F. Heinrich, S. Shenoy, M. Losche, D.J. Vanderah, Structure and properties of tethered bilayer lipid membranes with unsaturated anchor molecules, Langmuir 29 (2013) 8645–8656.
[34] M. Brzozowska, B.P. Oberts, G.J. Blanchard, J. Majewski, P. Krysinski, Design and characterization of novel tether layer for coupling of a bilayer lipid membrane to the surface of gold, Langmuir 25 (2009) 9337–9345.
[35] V. Atanasov, P.P. Atanasova, I.K. Vockenroth, N. Knorr, I. Koper, A molecular toolkit for highly insulating tethered bilayer lipid membranes on various substrates, Bioconjug. Chem. 17 (2006) 631–637.
[36] P. Theato, R. Zentel, Formation of lipid bilayers on a new amphiphilic polymer support, Langmuir 16 (2000) 1801–1805.
[37] M.L. Wagner, L.K. Tamm, Tethered polymer-supported planar lipid bilayers for reconstitution of integral membrane proteins: silane-polyethyleneglycol-lipid as a cushion and covalent linker, Biophys. J. 79 (2000) 1400–1414.
[38] B.A. Cornell, V.L.B. BraachMaksvytis, L.G. King, P.D.J. Osman, B. Raguse, L. Wieczorek, R.J. Pace, A biosensor that uses ion-channel switches, Nature 387 (1997) 580–583.
[39] D.J. McGillivray, G. Valincius, D.J. Vanderah, W. Febo-Ayala, J.T. Woodward, F. Heinrich, J.J. Kasianowicz, M. Losche, Molecular-scale structural and functional characterization of sparsely tethered bilayer lipid membranes, Biointerphases 2 (2007) 21–33.
[40] A. Junghans, I. Koper, Structural analysis of tethered bilayer lipid membranes, Langmuir 26 (2010) 11035–11040.
[41] I.K. Vockenroth, C. Ohm, J.W.F. Robertson, D.J. McGillivray, M. Losche, I. Koper, Stable insulating tethered bilayer lipid membranes, Biointerphases 3 (2008) FA68–FA73.
[42] R. Budvytyte, M. Mickevicius, D.J. Vanderah, F. Heinrich, G. Valincius, Modification of tethered bilayers by phospholipid exchange with vesicles, Langmuir 29 (2013) 4320–4327.
[43] H. Basit, A. Van der Heyden, C. Gondran, B. Nysten, P. Dumy, P. Labbe, Tethered bilayer lipid membranes on mixed self-assembled monolayers of a novel anchoring thiol: impact of the anchoring thiol density on bilayer formation, Langmuir 27 (2011) 14317–14328.
[44] S. Lingler, I. Rubinstein, W. Knoll, A. Offenhausser, Fusion of small unilamelar lipid vesicles to alkanethiol and thiolipid self-assembled monolayers on gold, Langmuir 13 (1997) 7085–7091.
[45] S.A. Glazier, D.J. Vanderah, A.L. Plant, H. Bayley, G. Valincius, J.J. Kasianowicz, Reconstitution of the pore-forming toxin alpha-hemolysin in phospholipid/18-octadecyl-1-thiahexa(ethylene oxide) and phospholipid/n-octadecanethiol supported bilayer membranes, Langmuir 16 (2000) 10428–10435.
[46] I.K. Vockenroth, C. Rossi, M.R. Shah, I. Koper, Formation of tethered bilayer lipid membranes probed by various surface sensitive techniques, Biointerphases 4 (2009) 19–26.
[47] I.K. Vockenroth, P.P. Atanasova, A.T.A. Jenkins, I. Koper, Incorporation of alpha-hemolysin in different tethered bilayer lipid membrane architectures, Langmuir 24 (2008) 496–502.
[48] G. Valincius, T. Meskauskas, F. Ivanauskas, Electrochemical impedance spectroscopy of tethered bilayer membranes, Langmuir 28 (2012) 977–990.
[49] D.D. Lasic, The mechanism of vesicle formation, Biochem. J. 256 (1988) 1–11.
[50] W. Helfrich, Lyotropic lamellar phases, J. Phys. Condens. Matter 9 (1994) A79–A92.
[51] B. Rakovska, T. Ragaliauskas, M. Mickevicius, M. Jankunec, G. Niaura, D.J. Vanderah, G. Valincius, Structure and function of the membrane self-assembled monolayers, Langmuir 31 (2015) 846–857.
[52] F. Heinrich, M. Lösche, Zooming in on disordered systems: neutron reflection studies of proteins associated with fluid membranes, Biochim. Biophys. Acta, Biomembr. 1838 (2014) 2341–2349.
[53] D.J. McGillivray, G. Valincius, F. Heinrich, J.W.F. Robertson, D.J. Vanderah, W. Febo-Ayala, I. Ignatjev, M. Losche, J.J. Kasianowicz, Structure of functional *Staphylococcus aureus* alpha-hemolysin channels in tethered bilayer lipid membranes, Biophys. J. 96 (2009) 1547–1553.
[54] G. Valincius, M. Mickevicius, Tethered phospholipid bilayer membranes: an interpretation of the electrochemical impedance response, in: A. Iglič (Ed.) Advances in Planar Lipid Bilayers and Liposomes, vol. 21, Elsevier 2015, pp. 27–61.
[55] J.A. de Feijter, J. Benjamins, F.A. Veer, Ellipsometry as a tool to study the adsorption of synthetic and biopolymers at the air-water interface, Biopolymers 17 (1978) 1759–1772.
[56] A. Erbe, R. Sigel, Tilt angle of lipid acyl chains in unilamellar vesicles determined by ellipsometric light scattering, Eur. Phys. J. E 22 (2007) 303–309.
[57] S. Tristram-Nagle, H.I. Petrache, J.F. Nagle, Structure and interactions of fully hydrated dioleoylphosphatidylcholine bilayers, Biophys. J. 75 (1998) 917–925.
[58] L. Ringstad, E. Protopapa, B. Lindholm-Sethson, A. Schmidtchen, A. Nelson, M. Malmsten, An electrochemical study into the interaction between complement-derived peptides and DOPC mono- and bilayers, Langmuir 24 (2008) 208–216.
[59] G. Preta, M. Jankunec, F. Heinrich, S. Griffin, I.M. Sheldon, G. Valincius, Tethered bilayer membranes as a complementary tool for functional and structural studies: the pyolysin case, Biochim. Biophys. Acta, Biomembr. 1858 (9) (2016) 2070–2080, http://dx.doi.org/10.1016/j.bbamem.2016.05.016.
[60] K.J. Kwak, G. Valincius, W.C. Liao, X. Hu, X.J. Wen, A. Lee, B. Yu, D.J. Vanderah, W. Lu, L.J. Lee, Formation and finite element analysis of tethered bilayer lipid structures, Langmuir 26 (2010) 18199–18208.
[61] T.N. Tun, A.T.A. Jenkins, An electrochemical impedance study of the effect of pathogenic bacterial toxins on tethered bilayer lipid membrane, Electrochem. Commun. 12 (2010) 1411–1415.
[62] L. Becucci, R. Guidelli, Q.Y. Liu, R.J. Bushby, S.D. Evans, A biomimetic membrane consisting of a polyethyleneoxythiol monolayer anchored to mercury with a phospholipid bilayer on top, J. Phys. Chem. B 160 (2002) 10410–10416.
[63] Y.J. Jing, H. Trefna, M. Persson, B. Kasemo, S. Svedhem, Formation of supported lipid bilayers on silica: relation to lipid phase transition temperature and liposome size, Soft Matter 10 (2014) 187–195.